Soft Matter

PAPER

View Article Online
View Journal | View Issue

Cite this: *Soft Matter*, 2026, **22**, 4007

Transient negative capacitance in ferroelectric and twist-bend ferroelectric nematic liquid crystals

Netra Prasad Dhakal,[ab] Manisha Talwar,[ac] Zakaria Siddiquee,[ac] Jakub Karcz,[d] Przemysław Kula,[d] Peter Salamon[e] and Antal Jákli *[abc]

The negative capacitance (NC) of ferroelectric materials can be used in conventional electronics to reduce power dissipation. Recently, NC was shown (N. P. Dhakal, A. Adaka, R. J. Twieg, N. A. Clark and A. Jákli, *Phys. Rev. Appl.*, 2025, **24**, 014029, DOI: 10.1103/fjx3-jd2y) to exist in a fluid ferroelectric nematic (N_F) liquid crystal material as well. Studies presented in this paper strongly indicate that NC exists in all ferroelectric nematic liquid crystal materials provided that the polarization switching time is larger than the rise time of the applied square-wave voltage. Additionally, NC was studied in a recently discovered fluid twist-bend ferroelectric nematic liquid crystal (N_{TBF}) material while switching its ferroelectric polarization. In contrast to the 2 NC ranges found in conventional ferroelectric crystals and ferroelectric nematic liquid crystals, in the N_{TBF} phase, the polarization switching happens in two steps leading to four negative capacitance ranges in the *P*–*V* hysteresis curves. Our measurements and analyses also provide estimates of the rotational viscosities and the physical mechanisms of the polarization switching steps in the N_{TBF} phase.

Received 31st March 2026,
Accepted 5th May 2026

DOI: 10.1039/d6sm00284f

rsc.li/soft-matter-journal

I. Introduction

The capacitance (C) of a capacitor is given by $C = \frac{dQ}{dV}$, where Q is the charge stored on the electrodes and V is the voltage between them. The energy stored in a capacitor is $W = \frac{Q^2}{2C} = \frac{1}{2}QV$, which is positive for positive capacitance.[1,2] In a ferroelectric material with a spontaneous polarization $\vec{P}_s$, the electric displacement $\vec{D}$ that measures the free surface charge density on plates is $\vec{D} = \varepsilon_0\varepsilon_r\vec{E}_F + \vec{P}_s$. Here, $\varepsilon_0 = 8.85 \times 10^{-12}$ C^2 N^{-1} m^{-2} is the permittivity of a vacuum, ε_r is the relative dielectric permittivity of the material and $\vec{E}_F = \vec{E} - \frac{\vec{P}_s,}{\varepsilon_0\varepsilon_r}$ is the electric field in the ferroelectric material. This gives $\frac{\partial\vec{D}}{\partial\vec{E}_F} = \varepsilon_0\varepsilon_r + \frac{\partial\vec{P}_s}{\partial\vec{E}_F} = \varepsilon_0\varepsilon_r + \varepsilon_0\varepsilon_F$, where ε_F is the ferroelectric permittivity. While ε_r is always positive, ε_F can be negative if $\frac{\partial\vec{P}_s}{\partial\vec{E}_F} < 0$. This was discussed by Landau and Khalatnikov already in the early days of ferroelectricity.[3] According to the Landau–Ginzburg theory, the polarization dependence of the free energy density of a ferroelectric material in an electric field $E_F = |\vec{E}_F|$ can be written as $f = aP_s^2 + bP_s^4 - E_FP_s$,[4,5] where $a < 0$ and $b > 0$ are the Landau coefficients assuming a second order paraelectric–ferroelectric phase transition. This corresponds to a double-well function with stable polarization values at the minima and an unstable $P_s = 0$, as depicted in Fig. 1(a). Minimizing f with respect to P_s, we obtain the electric field (E_F) inside ferroelectric materials as $E_F = 2aP_s + 4bP_s^3$. The plot of P_s against E_F has an "S" shape (Fig. 1(b)). In this curve, the orange shaded thermodynamically unstable range represents $\varepsilon_F < 0$ where the polarization changes opposite to the electric field; therefore, the capacitance becomes negative.[6] In this range, E_F decreases while the average P_s increases (switching from the negative to the positive direction), *i.e.*, while the capacitor is charging.[6,7]

In addition to solid ferroelectric[8–10] and antiferroelectric[11,12] materials, transient negative capacitance (NC) has also been reported recently in several 3D fluid ferroelectric nematic liquid crystals (N_F).[13] N_F liquid crystals consist of highly polar molecules with dipole moments greater than 9*D*. When cooled from

[a] *Advanced Materials and Liquid Crystal Institute, Kent State University, Kent, OH 44242, USA. E-mail: ajakli@kent.edu*
[b] *Materials Science Graduate Program, Kent State University, Kent, OH 44242, USA*
[c] *Department of Physics, Kent State University, Kent, OH 44242, USA*
[d] *Faculty of Advanced Technology and Chemistry, Military University of Technology, Warsaw 00-908, Poland*
[e] *Institute for Solid State Physics and Optics, HUN-REN Wigner Research Centre for Physics, P.O. Box 49, Budapest H-1525, Hungary*

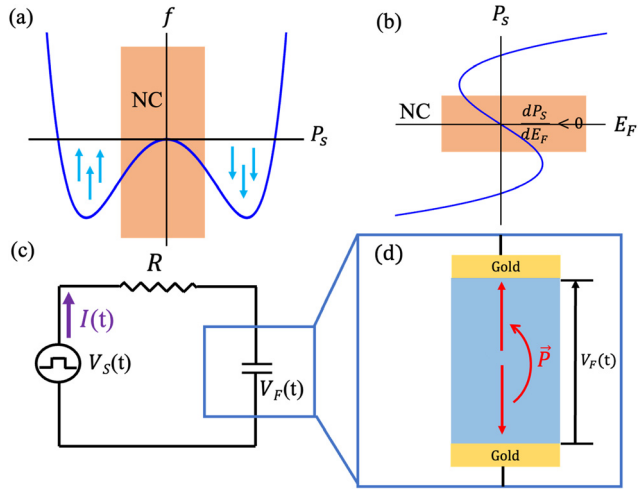

Fig. 1 Illustration of the principle and experimental realization of ferroelectric materials with transient negative capacitance. (a) Schematic free energy density f as a function of the ferroelectric polarization P_s of a ferroelectric material with a second order paraelectric–ferroelectric phase transition. (b) Ferroelectric polarization P_s as a function of the electric field in a ferroelectric material with $f(P_s)$ corresponding to (a). Orange shaded areas indicate unstable states. (c) Schematic representation of a measuring circuit consisting of an external voltage source V_S, and a resistance R connected in series with a ferroelectric capacitor. (d) Illustration of flipping of the polarization upon applying a square wave voltage $V_S(t)$ of the ferroelectric liquid crystal sandwiched between gold electrodes.

the paraelectric nematic phase (N) characterized by an averaged molecular direction ($\hat{n} = -\hat{n}$) (see Fig. 2(a)) to the ferroelectric nematic phase, these dipoles align along a particular direction breaking the inversion symmetry of the director ($\hat{n} \neq -\hat{n}$) and show spontaneous polarizations in the order of $P_s \sim 5$–$8\ \mu C\ cm^{-2}$

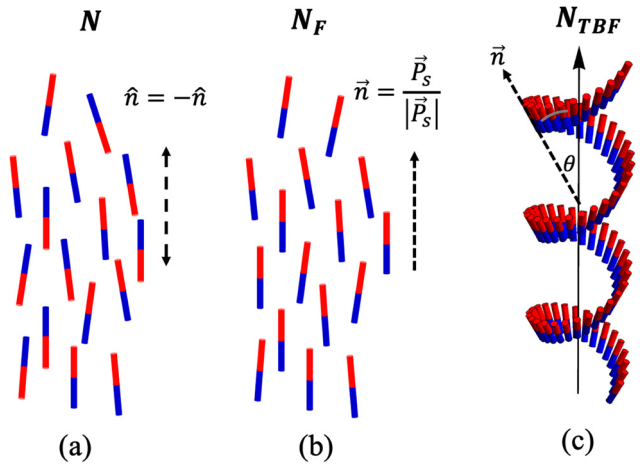

Fig. 2 Schematic illustration of nematic (N), ferroelectric nematic (N_F) and twist bend ferroelectric nematic (N_{TBF}) liquid crystal phases. Red (blue) parts indicate positively (negatively) charged areas forming molecular dipoles. (a) N phase, where an equal number of dipoles are pointing up, and (b) N_F phase, where most molecular dipoles point in the same direction leading to a spontaneous polarization $\vec{P}_s$ along the director $\vec{n}$; (c) N_{TBF} phase, where the director rotates around the helicoidal axis making an angle (θ) with the local polarization direction.

(ref. 14–17) (see Fig. 2(b)). In contrast to solid ferroelectrics where the polarization switched *via* boundary motion, in fluid ferroelectric LC, the polarization can rotate with respect to an axis normal to the electric field.[18,19] When a square wave electric field is applied through a series resistance R (Fig. 1(c)), the polarization flips following the direction of the applied voltage as illustrated in Fig. 1(d).[13,20–24] To observe NC, *i.e.*, a negative slope of the voltage drop across the ferroelectric fluid, P_s should rotate after the applied voltage has fully switched. The viscosity of the N_F material and therefore the switching time highly depend on the temperature.[25,26]

Previous experiments carried out in the geometry shown in Fig. 1(d) on several N_F materials found evidence for transient NC only in a room temperature N_F mixture with a relatively high rotational viscosity ($\gamma \approx 20$ Pa s) and failed to demonstrate it on the two high temperature prototypical N_F substances RM734[27] and DIO[16] with much smaller rotational viscosity values.

In this paper, we present redesigned studies on the low viscosity prototypical N_F materials and on a material having both an N_F phase and a ferroelectric twist bend nematic N_{TBF} phase.[28–31] The formation of the N_{TBF} phase is due to the competition between bend elasticity, molecular shape anisotropy, and polar interactions, resulting in a chiral symmetry breaking.[28,32] The vector of local spontaneous polarization follows an oblique helicoidal trajectory around a polar twist bend axis making a conical tilt angle θ (see Fig. 2(c)), which is similar to the previously reported dielectric twist bend nematic phase (N_{TB}).[33,34] Note that while the local polarization rotates around the helical axis, its component perpendicular to the helical axis is averaged out over one pitch, resulting in a decreased bulk polarization parallel to the helical axis. The pitch of the N_{TBF} phase is in the range from a few hundred nanometers[28,35] to a few micrometers.[36] When an electric field is applied in N_{TBF}, the polarizations rotate towards the electric field, and the cone angle decreases to allow the polarization to completely align along the field.[28,37]

We find strong evidence that NC is an inherent property of N_F materials, and it can be detected in all N_F (and any ferroelectric) materials provided that the rise time of the applied voltage V_S is smaller than the switching time of the polarization. We also show that NC can be detected even in the N_{TBF} phase, but instead of a single negative peak in the V_F, there are double negative peaks. We argue that this is due to the two-step polarization process related to the inversion of the heliconical axis and the field-induced decrease of the cone angle.

II. Materials and methods

Three compounds showing a ferroelectric nematic phase have been studied. The molecular structures and phase transition temperatures of two prototypical compounds, 4-[(4-nitrophenoxy)-carbonyl)] phenyl 2,4-dimethoxybenzoate (RM734)[27] and 2,3′,4′,5′-tetrafluoro[1,1′-biphenyl]-4-yl 2,6-difluoro-4-(5-propyl-1,3-dioxan-2-yl) benzoate (DIO),[38] are shown in Fig. 3(a) and (b). The chemical structure and phase transition temperatures of the substance

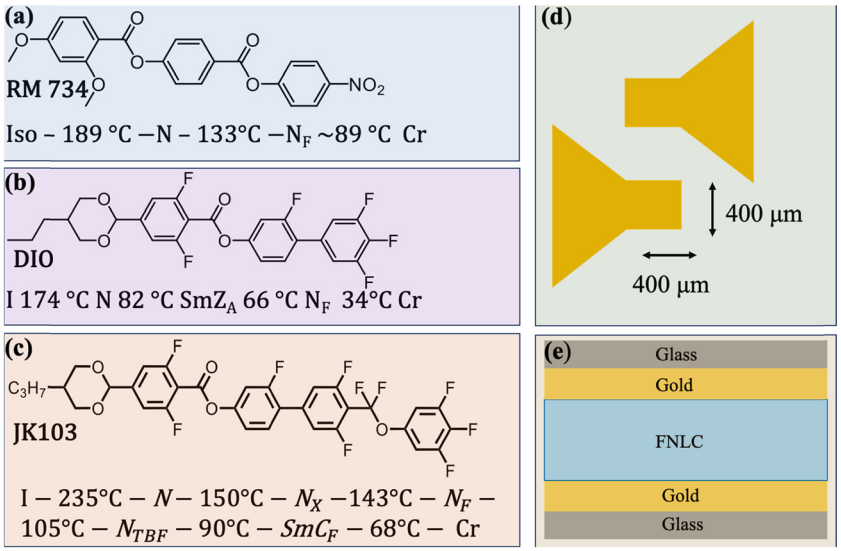

Fig. 3 Materials and methods. (a)–(c) Chemical structures and phase transition temperatures of the studied materials RM734, DIO and JK 103, respectively; (d) patterns of gold electrode on glass substrates overlapping across a 0.4 mm × 0.4 mm area; and (e) schematic cross section of the cell where the ferroelectric materials are sandwiched between gold electrodes covering the glass substrates.

4′-(difluoro(3,4,5-trifluorophenoxy)methyl)-2,3′,5′-trifluoro-[1,1′-biphenyl]-4-yl 2,6-difluoro-4-(5-propyl-1,3-dioxan-2-yl)benzoate (JK 103) are shown in Fig. 3(c). In addition to the N_F phase, JK103 also has a twist-bend ferroelectric N_{TBF} phase.[28]

All three materials are filled inside 20 µm cells by capillary action between gold patterned electrodes with 0.4 mm × 0.4 mm areas, as shown in Fig. 3(d) and (e). 100 Hz square wave voltages V_S generated using an Agilent 33120A function generator were applied between the gold electrodes. The time dependence of V_S is monitored in channel 1 of a Keysight 3024A oscilloscope. The liquid crystal (LC) cell is connected in series with a resistor R, and the voltage drop across the LC cell, V_F, is measured in channel 2 of the same oscilloscope. The role of the series resistor R is to adjust the charging of the capacitor by switching the ferroelectric polarization with time $\tau = RC$ of the liquid crystal cell (see Fig. 5c). To observe negative capacitance, it is important to have a larger polarization switching time than the rise time of the voltage, which necessitates the use of a square wave voltage. Identical cables are used for both channels, and the cable lengths are kept as short as possible to minimize parasitic effects.

III. Experimental results

Time dependences of the rectangular source voltage (V_S) and the ferroelectric voltage (V_F), measured using the circuit shown in Fig. 1(c), are seen for RM734 and DIO for various resistances in Fig. 4(a) and 5(a), respectively. After quickly switching V_S between ±2.5 V and ±1.5 V, V_F first changes sign, then reverses within 0.2 ms and ≈50 µs, then bounces back and saturates in about 2 ms and 0.5 ms for RM734 and DIO, respectively. Such a behavior is typical for ferroelectric[8–10] and antiferroelectric[11,12] crystals and was also found for a room temperature N_F[13] LC. Since the rotational viscosity of nematic LCs increases upon cooling, for both RM734 and DIO, the switching times increase with decreasing temperature (see Fig. 4(b) and 5(b)). The switching times determined by the peak positions in V_F are plotted in Fig. 4(c) and 5(c) with respect to the resistance R connected in series with the LC cells for RM734 and DIO, respectively. For both materials, the switching time is a linear function of R and the fitted lines intercept the x-axis at $R_i \approx -8$ kΩ and at $R_i \approx -12$ kΩ for RM734 and DIO, respectively. These values are close to that obtained for a room temperature N_F mixture[13] and the absolute values of R_i correspond to the resistance of the liquid crystal film ($|R_i| = R_{LC}$). In the entire N_F range of RM734 and DIO, the ohmic leakage current I_Ω is less than 5% of the ferroelectric polarization current as can be seen in Fig. 4a and 5a. Taking this into account, the ferroelectric polarization was calculated as $P(t) \approx \frac{\int (V_S(t) - V_F(t))dt}{RA} - \frac{\int I_C dt + \int I_\Omega dt}{A}$. The polarization as a function of voltage V_F is plotted in Fig. 4(d) and 5(d) for RM734 and DIO, respectively. Negative slopes indicated by light brown ellipses correspond to ranges with negative capacitance (NC). The saturated value of polarization for RM734 at 120 °C is $P_s \approx 0.055$ C m^{-2} and for DIO at 50 °C is $P \approx 0.04$ C m^{-2} in agreement with the literature values.[38,39]

A summary of the results obtained for 20 µm JK103 films in the N_F and N_{TBF} phases is shown in Fig. 6. Fig. 6(a) and (b) show the time dependences of V_F at various resistance values connected in series with the LC cell in comparison with the square wave source voltage of V_S = 2.2 V at 110 °C in the N_F phase and at 100 °C in the N_{TBF} phase, respectively. Our polarized optical microscopy observations revealed that at this source voltage, the sample goes to homeotropic indicating full polarization switching. Similar to the observations in RM734 and DIO, in

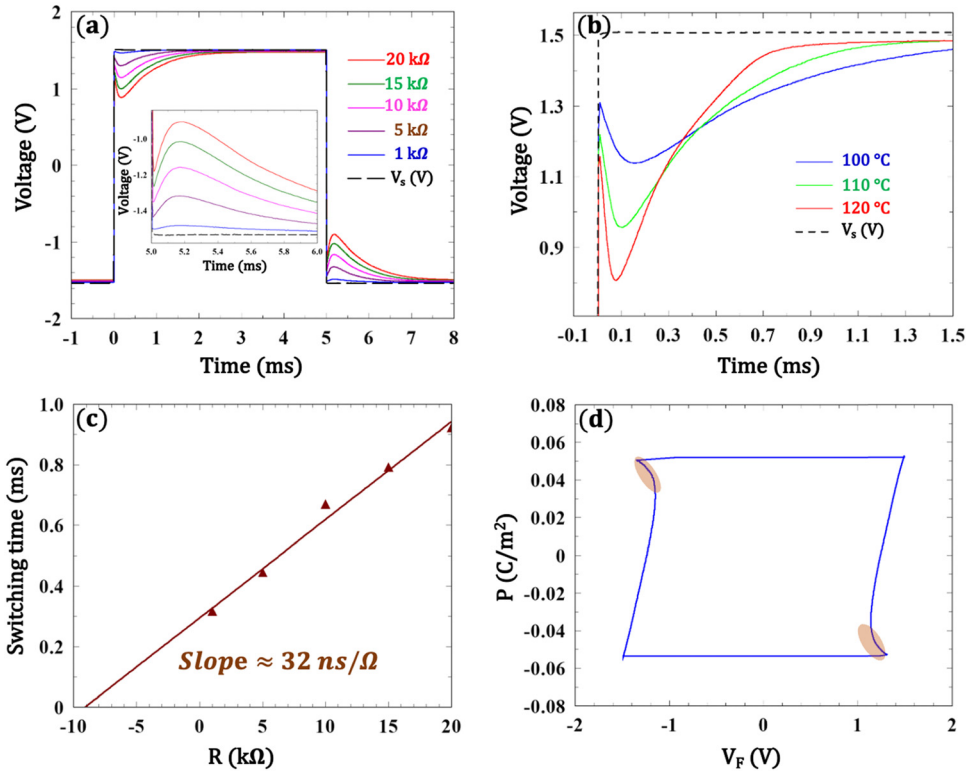

Fig. 4 Summary of the measurement results obtained on a 20 μm RM734 cell. (a) Time dependences of the rectangular source voltage (V_S) and the voltage dropping on the ferroelectric nematic liquid crystal film (V_F) for various resistances at 100 °C; (b) time dependence of V_S and V_F for resistance R = 10 kΩ at selected temperatures; (c) switching time with respect to R indicating linear behavior with slope ≈ 32 ns Ω^{-1} and intercept of the zero switching time at $R_i \approx -8$ kΩ; (d) polarization as a function of voltage V_F dropping on the ferroelectric LC film at 120 °C. Negative slopes indicated by light brown shapes correspond to ranges with negative capacitance (NC).

the N_F phase, V_F is decreasing (increasing) while V_S is increasing (decreasing) within 0.1 ms after the sign inversion of V_S, then bounces back and reaches an equilibrium value within 1 ms. In contrast to that found in the N_F phase, in the N_{TBF} phase the equilibrium is reached in two steps showing two peaks of $V_F(t)$ as shown in Fig. 6(b) at 100 °C.

The current going through the sample can be calculated as $I(t) = (V_S(t) - V_F(t))/R$. At R = 5 kΩ, $I(t)$ is shown in Fig. 6(c). The area $\int I_C dt$ below the capacitive decay current I_C corresponds to the capacitive charge $Q_C = C \cdot V_F = \varepsilon_0 \varepsilon_r \frac{A}{L} \cdot V_F$ and can be estimated as $Q_C \sim \frac{5 \times 10^{-5}\ \text{A} \times 2 \times 10^{-4}\ \text{s}}{2} \sim 5$ nC; with V_F ~2.5 V, L = 20 μm and A = 0.16 mm^2 it provides $\varepsilon_r(\sim 100\ \text{Hz}) \approx 2.5 \times 10^4$. As argued by Clark *et al.*[23] and verified experimentally,[24] such a high value is related to the capacitance of the insulating layer, which for conducting surfaces, such as gold in our case, is related to the thickness ($L_i \sim 1$ nm) of the anchored FNLC molecules. We note that for the $L \approx 3$ μm film with bare ITO layers, $\varepsilon_r(\sim 100\ \text{Hz}) \approx 4 \times 10^3$ was measured in ref. 28. Assuming similar $L_i \sim 1$ nm for gold and ITO surfaces and taking into account that in our case $L \approx 20$ μm, the ratio of the apparent dielectric constant measured by Karcz *et al.* and estimated by us is $\frac{25}{4} \approx 6.5 \approx \frac{20}{3} = 6.7$. Polarization charges Q_1 and Q_2 under peak 1 and peak 2 in (c) as a function of resistance applied in series with the LC cell are plotted in Fig. 6(d). Both Q_1 and Q_2 linearly decrease with the resistance R.

The switching times defined as the time positions of peak 1 and peak 2 (see Fig. 6(c)) as a function of R are shown in the N_F phase at 110 °C and at 100 °C in the N_{TB} phase (representing peak 1 and peak 2) in Fig. 6(e). The fastest switching with the least R dependence was found in the N_F phase (green data points in Fig. 6(e)). The switching time related to the first peak in N_{TBF} is about 40% larger at 100 °C than at 110 °C (blue data points in Fig. 6(e)). The switching time related to the 2nd peak in the N_{TBF} phase (red data points in Fig. 6(e)) is three times larger and it shows the strongest R dependence. Fitting the R-dependences by linear functions as for RM734 and DIO, the resistances at zero switching times can be approximated as $R_i \approx -64$, -62 and -38 kΩ for the green, blue and red data points, respectively. These values are much larger than the $R_i \approx -10$ Ω found for RM734 and DIO. We note that in this case, the best fits are not the linear functions, but those that intercept the x axis at $R_i \approx -20$, -12 and -20 kΩ for 110 °C in N_F, and the 1st and 2nd peak at 100 °C in the N_{TBF} phase, respectively.

Finally, Fig. 6(f) compares the P–V_F plots in the N_F and N_{TBF} phases, where $P = Q_P/A = (\int I_P dt)/A$. In both phases, the saturated polarization is $P_s \approx 0.04$ C m^{-2} in agreement with ref. 28. Additionally, while similar to that found for RM734 and DIO, there are two ranges (highlighted by light brown ellipses)

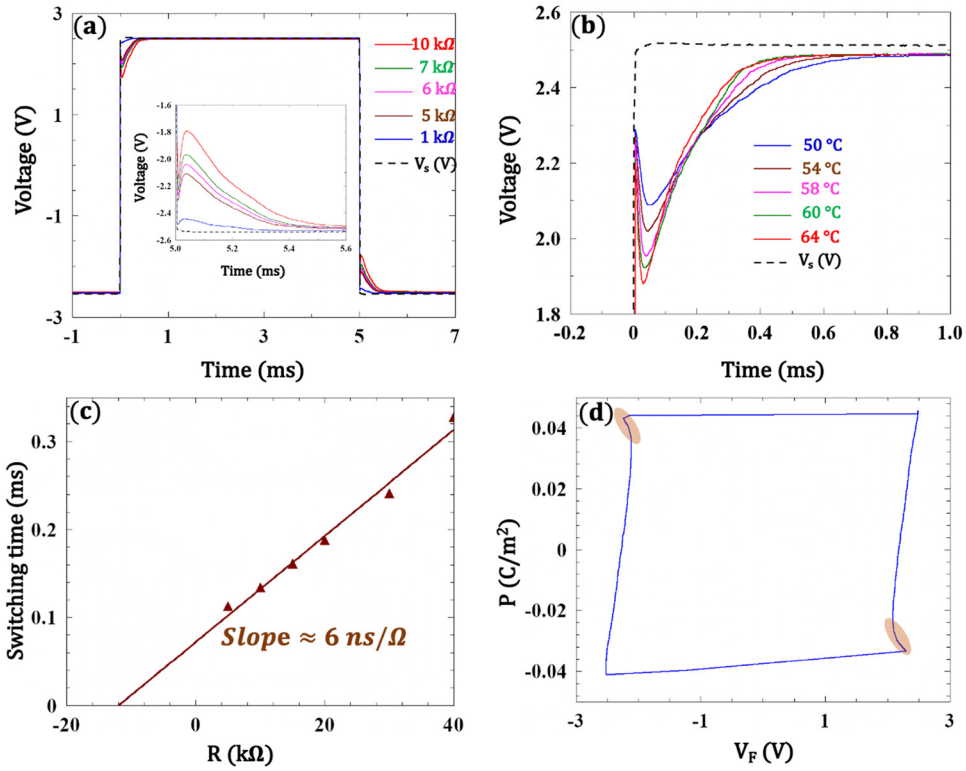

Fig. 5 Summary of the experimental results obtained on a 20 μm DIO cell. (a) Time dependences of the rectangular source voltage (V_S) and the voltage drop on the ferroelectric nematic liquid crystal film (V_F) for various resistances at 60 °C; (b) time dependence of V_S and V_F for resistance R = 7 kΩ at selected temperatures; (c) switching time with respect to R indicating linear behavior with slope ≈32 ns Ω^{-1} and intercept of the zero switching time at $R_i \approx -12$ kΩ; (d) polarization as a function of voltage V_F drop on the ferroelectric LC film at 50 °C. Negative slopes indicated by light brown shapes correspond to ranges with negative capacitance (NC).

showing NC in the N_F phase, and in the N_{TBF} phase there are 4 NC regions (highlighted by light blue ellipses). This is related to the double peaks seen in the N_{TBF} phase.

IV. Discussion

In previous results,[13] the transient capacitance (NC) could be shown in sandwich cells only for a room temperature N_F mixture with switching times around 1 ms under 5 V μm^{-1} fields. Here we showed similar NC also for the two prototypical N_F materials RM734 and DIO. Additionally (not discussed here), we have verified the presence of NC for all other (∼half a dozen) N_F materials that we have studied. This strongly indicates that all ferroelectric nematic liquid crystal (FNLC) materials have NC behavior. As it was argued previously, the necessary condition for the transient NC behavior is that the switching of the ferroelectric polarization be delayed compared to the rise time τ_r of the applied voltage V_S. The switching time of the polarization can be given as $\tau \approx \frac{\pi L \gamma}{P V_F}$,[23] where L is the film thickness, γ is the rotational viscosity of the material, and V_F is the voltage drop on the N_F LC. In previous measurements, the rise time was $\tau_r \approx 0.2$ ms, the film thickness was L = 4 μm and $V_F \leq 20$ V. This means that the rotational viscosity of the material had to be $\gamma \geq \frac{\tau_r P V_F}{\pi L} \approx 10$ Pa s. This was true only for the previously observed room temperature mixture KPA02 where $\gamma \approx 20$ Pa s, explaining why we could detect it only for that N_F LC material. In our present setup $\tau_r \approx 1$ μs and L = 20 μm, thus allowing us to measure NC in N_F LCs with $\gamma \geq 2$ mPa s. The rotational viscosities of the studied FNLC compounds can be calculated from the intercepts R_i of the linear fits of the $\tau(R)$ functions as shown for RM734 and DIO in Fig. 4(c) and 5(c), respectively. Since $|R_i| = R_{LC} = \frac{L \cdot \gamma}{A P^2}$,[13] from R_{LC} = 8 kΩ for RM734 with $P_s \approx 6$ μC cm^{-2} and R_{LC} = 12 kΩ for DIO with $P_s \approx 4.5$ μC cm^{-2}, we get that $\gamma \approx 0.23$ Pa s for RM734 at 100 °C, and $\gamma \approx 0.21$ Pa s for DIO at 60 °C. These values are indeed measurable by our method and are reasonable.

In addition to verifying the required experimental conditions to measure NC in FNLCs, the other significant result of our work is the observation of the double current peak in the N_{TBF} phase of JK103. This is in contrast to previous polarization measurements where only single polarization current peaks were observed in the N_{TBF}[28,31,37] of the same JK103 phase and in the so called $^{HC}N_F$.[32] We note, however, that an indication of double polarization peaks was observed in the tilted helical smectic SmC_P^H phase of JK103[37] and in the N_{TBF} and HEC phases of another ferroelectric nematic substance.[32,40] The

peak forming at decreasing fields was assigned to the increase of the heliconical angle θ from zero to the equilibrium value θ_0, whereas the peak that appears at increasing fields was assigned to the polarization flipping between $-P_s \cos\theta_0$ and $+P_s \cos\theta_0$ values.

In our measurements, we have observed the two peaks under rectangular fields, and thus we distinguish them by the switching times and not by the switching voltages. To find out the underlying physical mechanisms of these peaks, in addition to the positions of the fitted Gaussian peaks seen in Fig. 6(c), we also measured the areas representing the polarization charges Q_1 and Q_2 under these peaks, as shown in Fig. 6(d). Both Q_1 and Q_2 decrease with R, and their sum is decreasing from $Q_1 + Q_2 \approx 7$ nC at 5 kΩ to $Q_1 + Q_2 \approx 4.2$ nC at 51 kΩ. This is likely because V_F is decreasing at increasing R, *i.e.*, less voltage will drop on the sample. Fig. 6(a) shows that when $R = 51$ kΩ, V_F decreases from 2.2 V to 2.05 V at 110 °C in the N_F phase and to 2.1 V at 100 °C in the N_{TBF} phase. In fact, taking into account these values and the geometry of the films ($L = 20$ μm and $A = 0.16$ mm^2), we get for the DC conductivity values that $\sigma_{DC} = 1.8 \times 10^{-9}$ (Ω m)$^{-1}$ at 110 °C and $\sigma_{DC} = 1.3 \times 10^{-9}$ (Ω m)$^{-1}$ at 100 °C. As $V_s = 2.2$ V was chosen such that it was

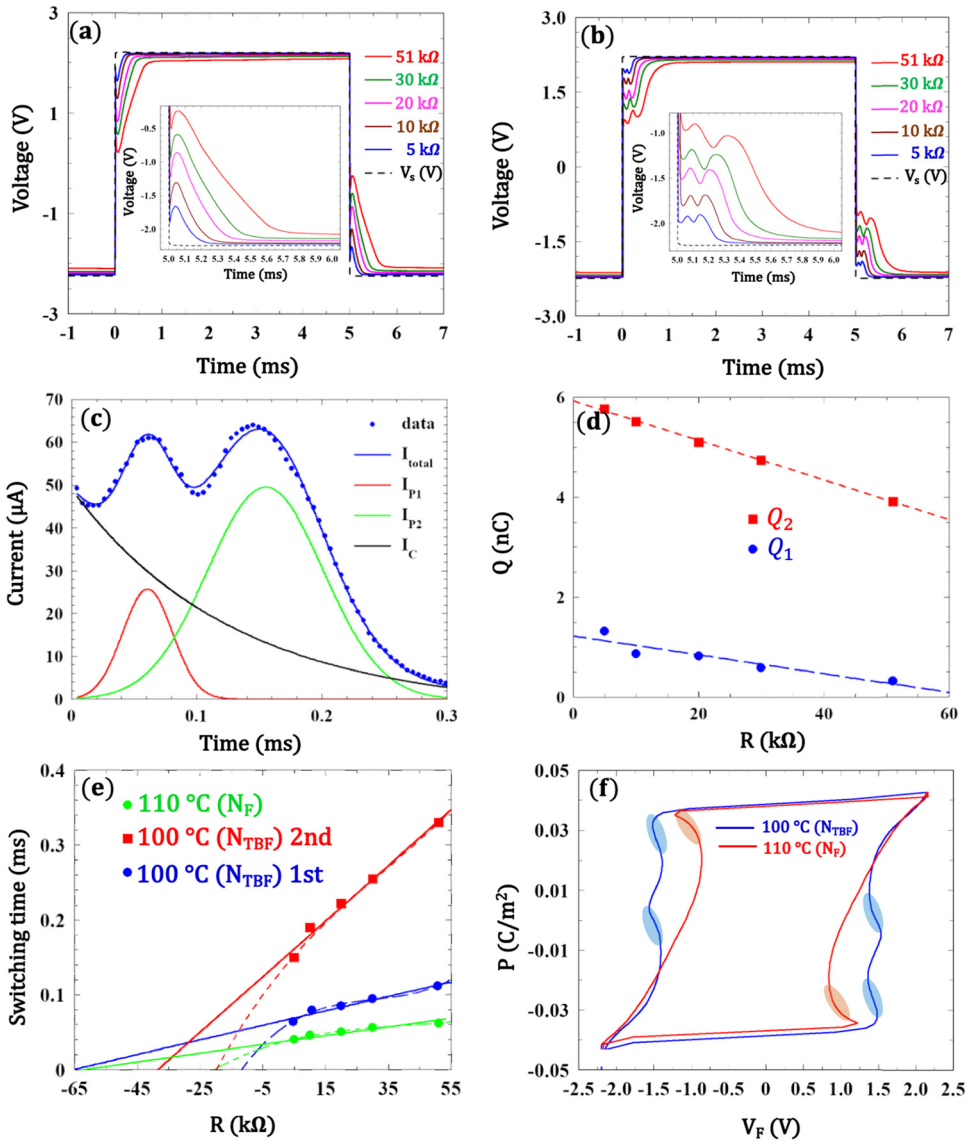

Fig. 6 Summary of the results obtained for a 20 μm JK103 cell. (a) Time dependences of the rectangular source voltage (V_S) and the voltage drop on the ferroelectric nematic liquid crystal film (V_F) for various resistances in the N_F phase at 110 °C; (b) time dependences of the rectangular source voltage (V_S) and the voltage drop on the ferroelectric nematic liquid crystal film (V_F) for various resistance in the N_{TBF} phase at 100 °C; (c) time dependence of the current for $R = 5$ kΩ; (d) polarization charges Q_1 and Q_2 under peak 1 and peak 2 in (c) as a function of resistance applied in series with the LC cell. (e) Switching times (defined as the time positions of the fitted current peaks in (c)) with respect to R at 110 °C (green dots) and at 100 °C related to the first peak (blue dots) and for the 2nd peak (red squares). Linear fits intercept the horizontal axis at $R_i = -64$, 62 and 38 kΩ for the green, blue and red data points, respectively. (f) P–V_F plots in the N_F and N_{TBF} phases. light brown and light blue ellipses show NC ranges in the N_F phase and N_{TBF} phase, respectively.

just slightly above the full polarization switching value when no resistance was connected in series to the LC film, even a small decrease in V_F when a resistance is in series leads to incomplete polarization switching. This may also explain the R dependences of the ratios of peak areas Q_2/Q_1 that increase from 4.4 at R = 5 kΩ to 12.6 at R = 51 kΩ. The variation of the charge involved in the flipping of the polarization between $-P_s \cos\theta_0$ and $+P_s \cos\theta_0$ is $Q_f = 2P_s \cos\theta_0$, while the one involved in the change of the cone angle from θ_0 to 0 is $Q_\theta = 2P_s(1 - \cos\theta_0)$. Assuming that the cone angle is smaller than 45°, we conclude that $Q_f = Q_2$ and $Q_\theta = Q_1$. A schematic representation of the polarization switching mechanisms involving variation of the cone angle (θ-mode) and flipping of the polarization (P-flip) leads to two current peaks as shown in Fig. 7. This is in accordance with the model of Gibb *et al.*[41] Note that polarization rotations corresponding to the increase and decrease of the tilt result in only one peak characterized by one switching time. The second peak, corresponding to the polarization flip, has a different switching time, and thus that appears separately.

This means that $\cos\theta_0 = \frac{Q_2}{Q_1 + Q_2}$. From Fig. 6(d) this gives $\theta_0 \approx 34°$ at R = 5 kΩ and $\theta_0 \approx 22°$ at R = 51 kΩ. This may be interpreted as complete closing of the cone angle during switching at R = 5 kΩ and only partial closing between 34° and 12° at R = 51 kΩ. We note that the estimated $\theta_0 \approx 34°$ at 100 °C of JK103 is much larger than what was calculated by Basnet *et al.*[31] from birefringence data. This might be due to a pre-transitional conical structure in the N_F phase, which can be deduced from Fig. 6(a), which already shows a combination of two peaks even at 110 °C in the N_F phase. This indicates a non-zero pretransitional cone angle and zero-field distribution of the polarization direction. Another possible reason for the apparently larger cone-angle deduced from the switching current is the coupling between the polarization flipping and cone-angle (θ) variation. At the instant when a voltage large enough to fully switch the polarization along the field (for example under V_s = 2.2 V at R = 5 kΩ) is quickly reversed, the polarization remains in the wrong direction, which is energetically unfavorable. The faster θ-mode can reduce the free-energy by increasing the cone angle, thus decreasing the polarization value shown in the wrong direction. As the polarization starts flipping, θ will decrease and the cone closes when all the polarization is along the field, thus further decreasing the free energy (see Fig. 7). Such an interplay between the two switching modes likely explains why for JK103 the switching time is not strictly a linear function of the resistance R, as seen in Fig. 6(e).

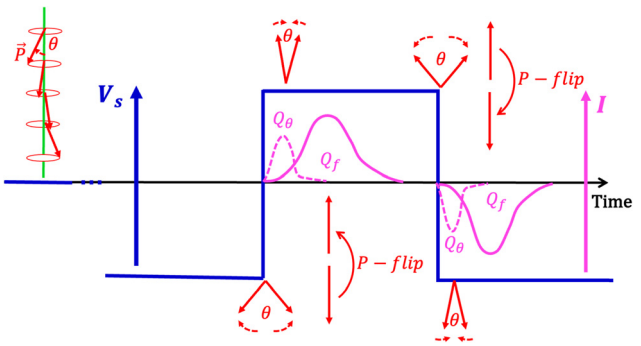

Fig. 7 Schematic representation of the polarization switching mechanisms involving variation of the cone angle (θ-mode) and flipping of the polarization (P-flip) leading to two current peaks. A sketch of the director structure at zero field is shown on the left side at a time before applying the square-wave voltage (blue lines). The polarization rotation and flipping during the switching are shown with red arrows and letters below and above the time-dependent voltage corresponding approximately to the time when they are happening. Pink curves and the pink vertical axis represent the time dependences of the electric current.

From the intercepts corresponding to the linear fit (solid lines in Fig. 6(e)), we can estimate the rotational viscosities γ corresponding to the polarization flipping both in the N_F and N_{TBF} phases and of γ_θ corresponding to the θ-mode in the N_{TBF} phase. In the N_F phase at 100 °C, taking $R_{LC} = \frac{L \cdot \gamma}{AP^2} \approx 64$ kΩ and with $L \approx 20$ μm, $A \approx 16 \times 10^4$ μm^2, and $P \approx 4.2 \times 10^{-2}$ C m^{-2}, we estimate that $\gamma \approx 0.82$ Pa s. This larger value than we found for RM734 and DIO at similar temperatures is likely due to the longer molecule of JK103. In the N_{TBF} phase at 100 °C, $R^f_{LC} = \frac{L \cdot \gamma}{AP^2 \cos^2\theta_0} \approx 38$ kΩ from the linear intercept (see Fig. 6(e)), which with $\theta_0 \approx 34°$ gives $\gamma \approx 0.34$ Pa s. This smaller value than in the higher temperature N_F phase makes sense, as now the flipping length is shorter due to the tilted polarization. From $R^\theta_{LC} = \frac{L \cdot \gamma}{AP^2(1 - \cos\theta_0)^2} \approx 62$ kΩ we get $\gamma_\theta \approx 0.14$ Pa s, which is smaller than γ as γ_θ involves smaller rotation of the director.

V. Conclusions

In this work, we have described the negative capacitance (NC) of two prototypical ferroelectric nematic liquid crystals RM734 and DIO. The presented results and additional studies on a number of other ferroelectric nematic liquid crystals in their N_F phase strongly suggest that all N_F materials show NC provided that the polarization switching time is larger than the rise time of the applied square-wave voltage.

Additionally, we have observed NC in one of the recently discovered fluid twist-bend ferroelectric nematic liquid crystal (N_{TBF}) materials JK103 while electrically switching its ferroelectric polarization. In contrast to two NC ranges found in conventional solid and fluid ferroelectric materials, in the N_{TBF} phase the polarization switching happens in two steps leading to four negative capacitance ranges in the P–V hysteresis curves. Our measurements and analyses also provided estimates of the rotational viscosities related to the flipping of the polarization (P-flip) and to the variation of the heliconical angle (θ-mode). Based on these results, we also provided models for these two switching mechanisms and explained similarities and differences between our and previous models.

Conflicts of interest

There are no conflicts to declare.

Data availability

The data supporting this study are available from the corresponding author upon reasonable request.

Acknowledgements

This work was financially supported by the US National Science Foundation grant DMR-2210083 and the Hungarian NKFIH FK142643.

References

1 L. D. Landau and I. M. Khalatnikov, *Dokl. Akad. Nauk*, 1954, **96**, 469–472.
2 J. Íñiguez, P. Zubko, I. Luk'yanchuk and A. Cano, *Nat. Rev. Mater.*, 2019, **4**, 243–256.
3 A. M. Bratkovsky and A. P. Levanyuk, *Appl. Phys. Lett.*, 2006, **89**(25), 253108.
4 P. Chandra and P. B. Littlewood, *Physics of Ferroelectrics: A Modern Perspective*, 2007, pp. 69–116.
5 M. Hoffmann, A. I. Khan, C. Serrao, Z. Lu, S. Salahuddin, M. Pešić, S. Slesazeck, U. Schroeder and T. Mikolajick, *J. Appl. Phys.*, 2018, **123**, 184101–184110.
6 M. Hoffmann, S. Slesazeck and T. Mikolajick, *APL Mater.*, 2021, **9**, 020902-1.
7 M. Hoffmann, P. V. Ravindran and A. I. Khan, *Materials*, 2019, **12**, 3743.
8 A. I. Khan, K. Chatterjee, B. Wang, S. Drapcho, L. You, C. Serrao, S. R. Bakaul, R. Ramesh and S. Salahuddin, *Nat. Mater.*, 2015, **14**, 182–186.
9 A. K. Yadav, K. X. Nguyen, Z. Hong, P. García-Fernández, P. Aguado-Puente, C. T. Nelson, S. Das, B. Prasad, D. Kwon, S. Cheema, A. I. Khan, C. Hu, J. Íñiguez, J. Junquera, L. Q. Chen, D. A. Muller, R. Ramesh and S. Salahuddin, *Nature*, 2019, **565**, 468–471.
10 M. Hoffmann, F. P. G. Fengler, M. Herzig, T. Mittmann, B. Max, U. Schroeder, R. Negrea, L. Pintilie, S. Slesazeck and T. Mikolajick, *Nature*, 2019, **565**, 464–467.
11 J. Doherty, K. A. Lynch and I. Ponomareva, *J. Appl. Phys.*, 2022, **132**, 034101.
12 M. Hoffmann, Z. Wang, N. Tasneem, A. Zubair, P. V. Ravindran, M. Tian, A. A. Gaskell, D. Triyoso, S. Consiglio, K. Tapily, R. Clark, J. Hur, S. S. K. Pentapati, S. K. Lim, M. Dopita, S. Yu, W. Chern, J. Kacher, S. E. Reyes-Lillo, D. Antoniadis, J. Ravichandran, S. Slesazeck, T. Mikolajick and A. I. Khan, *Nat. Commun.*, 2022, **13**, 1228.
13 N. P. Dhakal, A. Adaka, R. J. Twieg, N. A. Clark and A. Jákli, *Phys. Rev. Appl.*, 2025, **24**, 014029, DOI: 10.1103/fjx3-jd2y.
14 X. Chen, E. Korblova, D. Dong, X. Wei, R. Shao, L. Radzihovsky, M. A. Glaser, J. E. Maclennan, D. Bedrov, D. M. Walba and N. A. Clark, *Proc. Natl. Acad. Sci. U. S. A.*, 2020, **117**, 14021–14031.
15 N. Sebastián, M. Čopič and A. Mertelj, *Phys. Rev. E*, 2022, **106**, 021001-1.
16 H. Nishikawa, K. Shiroshita, H. Higuchi, Y. Okumura, Y. Haseba, S. I. Yamamoto, K. Sago and H. Kikuchi, *Adv. Mater.*, 2017, **29**, 1702354.
17 P. Guragain, A. Ghimire, M. Badu, N. P. Dhakal, P. Nepal, J. T. Gleeson, S. Sprunt, R. J. Twieg and A. Jákli, *Mater. Horiz.*, 2025, **12**, 8153–8164.
18 B. Basnet, M. Rajabi, H. Wang, P. Kumari, K. Thapa, S. Paul, M. O. Lavrentovich and O. D. Lavrentovich, *Nat. Commun.*, 2022, **13**, 3932.
19 X. Chen, E. Korblova, M. A. Glaser, J. E. Maclennan, D. M. Walba and N. A. Clark, *Proc. Natl. Acad. Sci. U. S. A.*, 2021, **118**, e2104092118.
20 N. Vaupotič, T. Krajnc, E. Gorecka, D. Pociecha and V. Matko, *Liq. Cryst.*, DOI: 10.1080/02678292.2025.2484234.
21 M. A. Osipov, *Liq. Cryst.*, DOI: 10.1080/02678292.2025.2528729.
22 V. Matko, E. Gorecka, D. Pociecha, J. Matraszek and N. Vaupotič, *Phys. Rev. Res.*, 2024, **6**, L042017.
23 N. A. Clark, X. Chen, J. E. MacLennan and M. A. Glaser, *Phys. Rev. Res.*, 2024, **6**, 013195.
24 A. Adaka, M. Rajabi, N. Haputhantrige, S. Sprunt, O. D. Lavrentovich and A. Jákli, *Phys. Rev. Lett.*, 2024, **133**, 038101.
25 A. Paul, M. Paul, M. Badu, A. Ghimire, N. P. Dhakal, S. Sprunt, A. Jákli and J. T. Gleeson, *Materials*, 2025, **18**, 5496–5509.
26 H. Nishikawa, P. Salamon, M. T. Máthé, A. Jákli and F. Araoka, *Giant*, 2025, **22**, 100356.
27 R. J. Mandle, S. J. Cowling and J. W. Goodby, *Phys. Chem. Chem. Phys.*, 2017, **19**, 11429–11435.
28 J. Karcz, J. Herman, N. Rychłowicz, P. Kula, E. Górecka, J. Szydlowska, P. W. Majewski and D. Pociecha, *Science*, 2024, **384**, 1096–1099.
29 P. Kumari, B. Basnet, M. O. Lavrentovich and O. D. Lavrentovich, *Science*, 2024, **383**, 1364–1368.
30 A. B. Szukalska, J. Karcz, J. Herman, D. Pociecha, E. Górecka, P. Kula and J. Myśliwiec, *Adv. Mater.*, 2026, **38**, e11648.
31 B. Basnet, P. Kumari, S. Paladugu, D. Pociecha, J. Karcz, P. Kula, N. Vaupotič, E. Górecka and O. D. Lavrentovich, *Adv. Sci.*, 2025, e15752.
32 H. Nishikawa, D. Okada, D. Kwaria, A. Nihonyanagi, M. Kuwayama, M. Hoshino and F. Araoka, *Adv. Sci.*, 2024, **11**, 2405718.
33 D. Chen, J. H. Porada, J. B. Hooper, A. Klittnick, Y. Shen, M. R. Tuchband, E. Korbloèa, D. Bedrov, D. M. Walba, M. A. Glaser, J. E. Maclennan and N. A. Clark, *Proc. Natl. Acad. Sci. U. S. A.*, 2013, **110**, 15931–15936.
34 V. Borshch, Y.-K. Kim, J. Xiang, M. Gao, A. Jakli, V. P. Panov, J. K. Vij, C. T. Imrie, M. G. Tamba, G. H. Mehl and O. D. Lavrentovich, *Nat. Commun.*, 2013, **4**, 2635-1-8.
35 G. J. Strachan, E. Górecka and D. Pociecha, *Mater. Horiz.*, 2026, **13**, 779.
36 G. J. Strachan, E. Górecka, J. Hobbs and D. Pociecha, *J. Am. Chem. Soc.*, 2025, **147**, 6058–6066.

37 J. Hobbs, C. J. Gibb and R. J. Mandle, *Nat. Commun.*, 2025, **16**, 7510.
38 H. Nishikawa, K. Shiroshita, H. Higuchi, Y. Okumura, Y. Haseba, S. I. Yamamoto, K. Sago and H. Kikuchi, *Adv. Mater.*, 2017, **29**, 1702354.
39 X. Chen, E. Korblova, D. Dong, X. Wei, R. Shao, L. Radzihovsky, M. A. Glaser, J. E. Maclennan, D. Bedrov, D. M. Walba and N. A. Clark, *Proc. Natl. Acad. Sci. U. S. A.*, 2020, **117**, 14021–14031.
40 H. Nishikawa, D. Kwaria, A. Nihonyanagi and F. Araoka, *Adv. Mater.*, 2025, **38**, e13451.
41 C. J. Gibb, J. Hobbs, D. I. Nikolova, T. Raistrick, S. R. Berrow, A. Mertelj, N. Osterman, N. Sebastián, H. F. Gleeson and R. J. Mandle, *Nat. Commun.*, 2024, **15**, 5845.